PCCP

RSC Publishing

PAPER

View Article Online
View Journal | View Issue

Cite this: *Phys. Chem. Chem. Phys.*, 2013, **15**, 16515

Electron transfer with azurin at Au–SAM junctions in contact with a protic ionic melt: impact of glassy dynamics†

Dimitri E. Khoshtariya,*[abcd] Tina D. Dolidze,[abc] Tatyana Tretyakova,[ab] David H. Waldeck[d] and Rudi van Eldik*[a]

Received 4th May 2013,
Accepted 24th July 2013

DOI: 10.1039/c3cp51896e

www.rsc.org/pccp

Gold electrodes were coated with alkanethiol SAM–azurin (Az, blue cupredoxin) assemblies and placed in contact with a water-doped and buffered protic ionic melt as the electrolyte, choline dihydrogen phosphate ([ch][dhp]). Fast-scan protein-film voltammetry was applied to explore interfacial biological electron transfer (ET) under conditions approaching the glass-transition border. The ET rate was studied as a function of the water amount, temperature (273–353 K), and pressure (0.1–150 MPa). Exposure of the Az films to the semi-solid electrolyte greatly affected the protein's conformational dynamics, hence the ET rate, *via* the mechanism occurring in the extra complicated dynamically-controlled regime, is compared to the earlier studies on the reference system with a conventional electrolyte (D. E. Khoshtariya *et al.*, *Proc. Natl. Acad. Sci. U. S. A.*, 2010, **107**, 2757–2762), allowing for the disclosure of even more uncommon mechanistic motifs. For samples with low water content (*ca.* 3 or less waters per [ch][dhp]), at moderately low temperatures (below *ca.* 298 K) and/or high pressure (150 MPa), the voltammetric profiles systematically deviated from the standard Marcus current–overvoltage pattern, deemed as attributable to a breakdown of the linear response approximation through the essential steepening of the Gibbs energy wells near the glass-forming threshold. Electrolytes with a higher water content (6 to 15 waters per [ch][dhp]) display anomalous temperature and pressure performances, suggesting that the system crosses a broad nonergodic zone which arises from the interplay of ET-coupled large-scale conformational (highly cooperative) modes of the Az protein, inherently linked to the electrolyte's (water-doped [ch][dhp]) slowest collective relaxation(s).

Introduction

Interfacial biological electron transfer (ET) involving the Au–SAM-deposited small redox proteins (Au, gold; SAM, self-assembled monolayer), partly immersed in conventional liquid phase electrolytes, has been studied extensively in the past.[1–14] While ET with 1 nm or thicker SAM spacers proceeds by a nonadiabatic mechanism, for thin SAM films[4,7,10–12,14] the ET rate seems to be determined by a dynamical control mechanism, hence controlled through the conformational relaxations occurring slowly over hundreds of nanoseconds.[4,10,14] Semi-solid conditions that normally offer a notable protein preservation, also raise some novel challenging mechanistic questions; hence a number of efforts were applied to explore the intrinsic links between the protein's dynamical and functional properties under solid-like conditions near the glass-forming threshold, from both fundamental[2,15–26] and applied[27–29] perspectives. However, systematic mechanistic studies of interfacial biological ET in glassy media by the standard voltammetry methods have been limited because of the poor solution conductivity of the semi-rigid environment and/or the extra-demanding cryogenic requirements. Fortunately, a number of protic ionic plastic crystals and their aqueous melts, including choline dihydrogen phosphate ([ch][dhp]), have been reported to possess significant ionic (particularly protic) conductance and remarkable bio-compatibility,[32–37] involvement of which, along with the enhancement of the stability and robustness of electroactive Au–SAM–protein assemblies, allows, on the one hand, to approach a solid-like (glassy) state under nearly ambient experimental conditions and, on the other hand, to warrant settings

[a] *Department of Chemistry and Pharmacy, University of Erlangen-Nürnberg, 91058 Erlangen, Germany. E-mail: vaneldik@chemie.uni-erlangen.de*
[b] *Institute for Biophysics and Bio-Nanosciences, Department of Physics, Tbilisi State University, 0128 Tbilisi, Georgia. E-mail: dimitri.khoshtariya@tsu.ge*
[c] *Department of Biophysics, Center for Experimental Biomedicine, 0160 Tbilisi, Georgia*
[d] *Department of Chemistry, University of Pittsburgh, Pittsburgh, PA 5260, USA. E-mail: dave@pitt.edu*

† Electronic supplementary information (ESI) available. See DOI: 10.1039/c3cp51896e

for obtaining the artifact-free, hence, fully reliable voltammetry data.

A semi-solid electrolyte may provide a more realistic mimic of the environment in a cell or biological membrane than does a simple aqueous electrolyte (see, *e.g.*, ref. 30 and 31). Hence, kinetic studies of such assemblies are highly relevant and may improve our understanding of electron transfer in biological organisms and structures. Furthermore, such fundamental studies may serve to advance applications; *e.g.* refine nanoscale design principles of certain bioelectronic devices.[27–29] Recent theoretical developments,[38–42] bringing together key notions of the basic ET theory[43–50] and complementary issues of the current soft matter physics,[51–53] jointly with recent findings from extensive computer simulations,[16,39,41,54,55] predict that different types of "irregularities" (deviations from the conventional kinetic motifs) can manifest as semi-rigid conditions are approached. Such irregularities may include:

• Nonergodic behavior (dynamically arrested ET) that is predicted to occur when the ET rate constant is varied over a range that is broad compared to the timescale of the system's relaxation modes, which contribute to the reaction rate.[18,38–42] The subsequent inability to draw clear timescale separations represents a breakdown in the underlying assumptions to the basic and extended Marcus models.[43–50] In experiments, this behavior can be manifested in a number of ways, including kinetic hysteresis (memory effects) and essentially curved (even upturned) Arrhenius motifs.[40–42,51–53]

• Nonlinearity in the solute–solvent coupling represents another breakdown in a basic assumption underlying the "classical" ET theory,[43–50] and it causes deviations from the familiar parabolic shapes of the reactant and product Gibbs energy profiles.[39–41,54,55]

Both these kinds of deviations have been theoretically conjectured[16,18,38–42,54,55] and experimentally well documented[42,56–58] (however, for a few ET processes in biological and chemical systems) under extremely viscous or semi-rigid conditions. In this study, we approach the glass-transition threshold by a dramatic reduction of the water content in the vicinity of a protein, and we compare the ET kinetics in this environment with that for a liquid-phase, aqueous electrolyte.[4,7,10–12,14]

This work explores interfacial biological ET in a protic electrolyte mixture that gradually extends over the liquid and semi-solid electrolyte conditions with a change in composition. The Au–SAM–Az assemblies (alkanethiol SAMs with methylene carbon numbers of 4 and 15; Az, azurin, blue cupredoxin) were placed in contact with a buffered protic ionic melt, [ch][dhp], containing from <2 to 15 water molecules per [ch][dhp] (content of the ionic component varied from 50 to 90% w/w), and the ET was studied as a function of temperature (273–353 K) and pressure (0.1–150 MPa) by fast-scan cyclic voltammetry. The extra confinement of the Az films within the highly rigidified environment affects the protein's conformational dynamics, hence the ET rate, *via* the mechanism occurring in a friction-controlled regime. The standard heterogeneous rate constants, k^0 (or k_{eff}), and respective reorganization free energies, λ_0 (λ_{eff}) were extracted from the voltammetry data through established procedures[59–62] (when applicable; see important caveats in the discussion below). These studies are unprecedented and reveal a remarkable interplay of the dynamically-controlled ET mechanism with accompanying nonergodic and nonlinear effects for biological ET.

Results and discussion

The CV data analysis

In liquid electrolytes, Marcus theory[43–45] and its basic extensions[46–50] are commonly used to describe electrochemical charge transfer rates in both the weak and strong electronic coupling limiting cases. In a general form, the reduction and oxidation rate constants, respectively, may be written as[60–62]

$$k_{\mathrm{red}}(\xi) = A\int \exp\left[-\frac{((\varepsilon_{\mathrm{F}}-\varepsilon)+e\xi+\lambda_0)^2}{4\lambda_0 RT}\right][f(\varepsilon)]\frac{\mathrm{d}\varepsilon}{RT} \qquad (1)$$

and

$$k_{\mathrm{ox}}(\xi) = A\int \exp\left[-\frac{((\varepsilon_{\mathrm{F}}-\varepsilon)-e\xi+\lambda_0)^2}{4\lambda_0 RT}\right][1-f(\varepsilon)]\frac{\mathrm{d}\varepsilon}{RT} \qquad (2)$$

In eqn (1) and (2), λ_0 is the reorganization energy, ξ is the overpotential (equal to the applied potential relative to the formal potential of the redox molecule), ε_{F} is the Fermi energy (equal to the applied potential), $f(\varepsilon)$ is the Fermi function, R is the gas constant, T is absolute temperature, and A is a pre-exponential factor whose form is specific for the intrinsic ET mechanism. The term ε is an integration variable that corresponds to the energy of the electronic levels in the electrode. In the overdamped, dynamically-controlled (DC) regime,[4,7,12,14,46–50,58,63–67] the pre-exponential factor can be written as:

$$A = A_{\mathrm{DC}} = \nu_{\mathrm{eff}}\sqrt{\frac{\lambda_{\mathrm{o}}}{\pi^3 RT}} \qquad (3)$$

where $\nu_{\mathrm{eff}} = 1/\tau_{\mathrm{eff}} \propto RT/\eta$,‡ [4,14,46–50,58,63–69] with ν_{eff} and τ_{eff} representing the effective frequency and relaxation time of the redox environment; under some circumstances τ_{eff} correlates well with the "microscopic" viscosity, η.[4,14,15,46–50,58,63–67] The standard electron-transfer rate constant, k^0, is obtained from either eqn (1) or (2). When the overpotential is zero and the ET is controlled by exchange at the electrode Fermi level, eqn (1) and (2) simplify to[43–45,59–62]

$$k^0 = A\exp\left(\frac{-\Delta G_{\mathrm{a}}}{RT}\right) \qquad (4)$$

where

$$\Delta G_{\mathrm{a}} = \frac{\lambda_{\mathrm{o}}}{4} - V_{\mathrm{AB}} \qquad (5)$$

In eqn (5), V_{AB} is the electronic coupling between the electron donor and acceptor states.[44–50]

Eqn (1) to (5) assume that the medium has a linear response corresponding to parabolic Gibbs energy profiles for the reactant and product states. The numerical solution of eqn (1) and

‡ Different models may differ by a numerical factor.

(2) allows for the accurate simulation of cyclic voltammograms at any value of the scan rate (v), rate constant (k^0), and reorganization Gibbs energy (λ_0).[60–62] The latter two parameters can then be determined through a numerical fitting procedure (overlay of experimental and theoretical curves), or by a comparison to voltammetric peak positions (relative to the formal potential) *versus* the scan rate.[60–62] For biological ET processes the value of λ_0, rather arbitrarily, can be considered as arising from several contributions due to the reorganization of: (a) the first coordination sphere of a metal core; (b) the rest of the protein interior and its interfacial zone; and (c) the external (bulk) medium.[13,14,45,63–65,70] The overall λ_0 can also be separated into contributions from the fast and slow reorganizable degrees of freedom (modes) that may belong either to the three above-mentioned specific zones (fast individual modes), or to two or three of them simultaneously (slow collective modes). Furthermore, the fast modes should be considered as statistically independent, non-dissipative and harmonic, while slow modes are believed to be cooperative, dissipative and, at least partially, unharmonic.[15,16,20,21,24–26,39–41,43–45,53–55,71] In the case of sluggish (viscous) environments, the slow modes of the protein's outer solution (*e.g.*, of the water-doped [ch][dhp] melt), of the protein's peripheral (interfacial) zone, and even of the protein's metal core neighborhood may be essentially coupled, and form hierarchical (intrinsically subordinated) set of connections (see the following sections for further discussion).[15,16,20,21,24–26,53–55,68–73] Accordingly, in the case of composite systems like ours, the classical Marcus relationship[43,45] for the outer-sphere component of the reorganization energy, $\lambda_{o(OS)} \propto [\epsilon_o^{-1} - \epsilon_s^{-1}]$ (where ϵ_o and ϵ_s are optical and static dielectric permittivity constants of the medium, respectively), is hardly applicable.[74,75] Anyway, the values of ϵ_o and ϵ_s, for choline-based PILs change little for respective binary mixtures above the [ch][dhp] mole fraction of *ca.* 0.3–0.4[76–78] (that is the range of our reported experimental work).

Fig. 1 shows some representative cyclic voltammograms for the electron exchange under different experimental conditions. For all the temperatures, pressures, and voltage sweep rates that were applied, the CVs displayed well-defined Faradaic redox peaks very similar to those reported previously with aqueous electrolytes.[10,14] However, they withstood the extremes of temperature (80 °C), pressure (150 MPa), and respective multiple temperature–pressure cycling much better than in the absence of [ch][dhp].[10,14] Actually, it was possible to approach the thermal stability threshold for a homogeneously dissolved native Az, 83 to 86 °C.[79] It has also been demonstrated before through Trp-48 fluorescence and phosphorescence emission studies that native Az in solutions withstood high pressures up to 300 MPa.[80] This was accompanied by a decrease of the protein's internal flexibility,[80] later shown to be manifested through the positive activation volume for a respective ET process.[10,14] Furthermore, it has been shown that the formal redox potential (E_o) of Az, within the pH range from 4 to 7, is practically unaffected by the immobilization at methyl-terminated SAMs (is virtually the same within experimental error for freely diffusing and irreversibly confined samples),[9,81] a result that could be expected for hydrophobically arrested proteins (including this particular case) provided that their secondary and tertiary structure is not destroyed (it remains native-like); even slight stabilization (*vs.* the impact of T and P) can be expected on general grounds. Simultaneously, convincing evidence of a native structure stabilization for Az and other enzymes by [ch][dhp] in solutions has been reported.[34–37] In line with all these findings, our present results including T and P cycling with control experiments at the end, also point to stability preservation of the immobilized Az protein up to 80 °C and/or 150 MPa, and to the remarkable stability increase of the SAM–Az assemblies in the presence of [ch][dhp], obviously thanks to the strengthening of the supramolecular hydrophobic interactions involved. Indeed, it seems extremely unlikely that these two independent, apparently stabilizing factors, acting together, could lead to a totally reversible destabilizing effect through the T and P cycling extremes.

Furthermore, Fig. 2, panels A and B, depict typical fittings for CV peak deviations at the experimental conditions under which the Marcus theory approximations hold. Hence, under some conditions (distinct [ch][dhp] concentrations, low pressure, moderately high temperature) the system behaves normally,

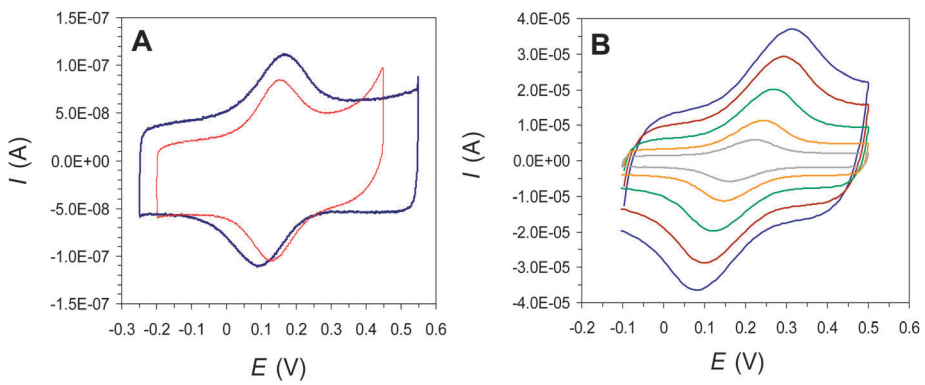

Fig. 1 (A) Typical CV records for the electron exchange of Azurin at a 1-pentanethiol (n = 4) SAM coated Au electrode placed in a 90% [ch][dhp] (w/w) aqueous buffered melt (pH 4.6), at T = 1 °C (thin curve), and T = 80 °C (bold curve); P = 0.1 MPa, potential scan rate: 0.1 V s^{-1}. (B) CV records for the electron exchange of Az at a like electrode in 70% [ch][dhp] solution (pH 4.6); T = 20 °C, P = 0.1 MPa; potential scan rates: 10, 20, 40, 60 and 80 V s^{-1} (the peak intensity increase).

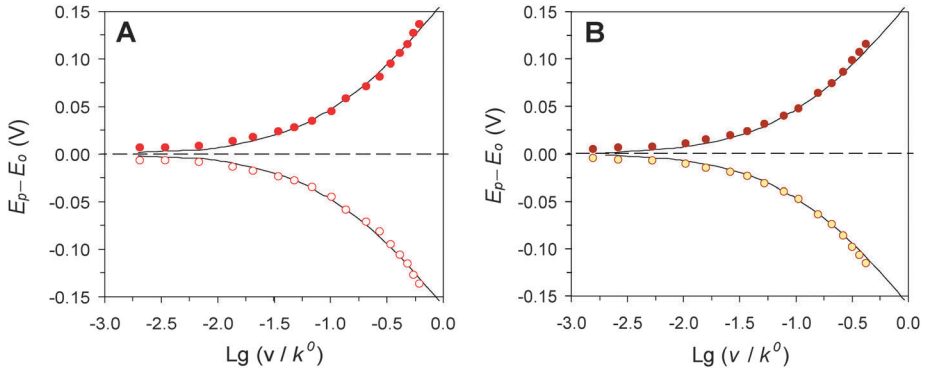

Fig. 2 Typical plots for the CV peak potential deviations (from the midpoint potential) as a function of the scaled scan rate (symbols) and their fits by the Marcus model (solid line) for two representative cases of an adequate resemblance: (A) the case of 85% [ch][dhp] aqueous buffered solution (pH 4.6); T = 50 °C; P = 150 MPa (before the abrupt transition; see the text), yielding the values: k^0 = 145 s^{-1}, λ = 0.3 eV. (B) The case of 70% [ch][dhp] aqueous buffered solution (pH 4.6); T = 20 °C; P = 0.1 MPa, yielding k^0 = 190 s^{-1}, λ = 0.3 eV.

apparently ergodic (regarding the temperature and pressure patterns, *vide infra*) and/or linearly responsive (that is, parabola-shaped regarding the free energy wells), as has been reported earlier for an aqueous, liquid electrolyte.[10,14] However, these experiments only probe the bottom segments of the energy wells, *ca.* 1.5 times the curve intercept point (≈0.075 eV), *vide infra*. In addition, Fig. 3, panels A and B, depict the cases where the data fitting follows the Marcus model only within a limited range of the given data series (see other subsections below).

The derivation of eqn (1) to (4) assumes that the solute–solvent coupling is linear and that the system is ergodic. For the situation of broken ergodicity, the reactive subsystem does not completely explore its phase space; *i.e.*, some modes are fast and contribute fully to the reorganization energy, while other modes are too slow (frozen) to contribute.[18,38,40] As a result, the apparent (effective) reorganization energy, λ_{eff}, can be smaller than the "full" (statistically equilibrated) value, λ_0[18,38,40,58] (however, see discussion below). Accordingly, while the physical parameters retain much of their physical meaning, the experimental values obtained for these parameters should be considered as "apparent" (statistically relative) rather than "true" (statistically well-justified) (see, *e.g.*, ref. 18, 38–42, 51–53 and 58). Despite the real progress in a general mechanistic understanding,[16,18,38–42] currently no well-established theoretical model is available to analyze the voltammetry in a quantitative manner under nonergodic and nonlinear conditions. Because we also explore regimes where these conditions appear to hold (at least within the overpotential and time domains of respective experiments, see *e.g.*, ref. 53), we can use the conventional models to describe the data in this limit (see ref. 18 and 38–42). Although the validity of eqn (1) to (5) is circumspect in the nonergodic regime, their application to the data provides a useful way to identify the conditions (composition, temperature, and pressure) under which clear deviations from the expected behavior are manifested. Thus we use eqn (1) to (5) to examine the data and identify the limits for which their description of the data fails.

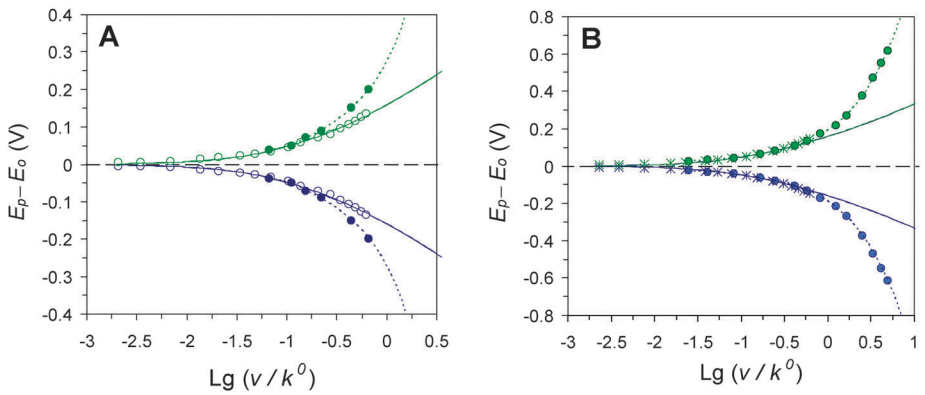

Fig. 3 Similar plots for two representative cases of a deficient (incomplete) fitting by the Marcus model: (A) the case of 85% [ch][dhp] aqueous buffered solution (pH 4.6) at T = 50 °C and P = 150 MPa, before and after the abrupt glassy transition (see the text). The open symbols are the same as in Fig. 2, panel A (with parameters already indicated there); the closed symbols depict the situation after the transition, allowing a partial fitting below the overpotential of 0.1 V (yielding: k^0 = 4.5 s^{-1}, λ = 0.3 eV). Note, above this potential, the data could not be fitted by any Marcus curve; the dotted curves are drawn to guide the eye only. (B) The case of 90% [ch][dhp] aqueous buffered solution (pH 4.6), recorded at P = 0.1 MPa (ambient pressure); T = 80 °C (asterisks) and 20 °C (closed circles). At T = 80 °C, the Marcus model fits yield k^0 = 130 s^{-1} and λ = 0.3 eV, while, at T = 20 °C below the overpotential of *ca.* 0.15 V, the Marcus fit yields k^0 = 12 s^{-1} and λ = 0.3 eV. Note, the data collected at 20 °C above *ca.* 0.15 V could not be fitted by any curve of the Marcus model; the dotted curves are drawn to guide the eye only (see text and ESI† for more details).

The impact of temperature and pressure

The friction-controlled regime manifests itself, in part, by an additional enthalpy (volume) of activation that arises from the temperature (pressure) dependence of the parameter ν_{eff} and respective positive volume of activation that is typical of diffusional and quasi-diffusional (friction-controlled) processes in soft matter.[10,14,49–51,66–68] Hence, consideration of the temperature and pressure effects on k^0, λ_{eff} and ν_{eff} helps to outline the entire picture of an impact of the medium's gradual solidification on biological ET, and to find physical conditions at which the anomalous motifs start to show up. This, in turn, will facilitate developments to match theoretical investigations. Under conditions where ergodicity is not broken, the dependence of $\ln(k^0)$ on T^{-1} provides the activation enthalpy[10,14,43–45,58,66,67] *via* eqn (6),

$$\left[\frac{\partial(\ln k^0)}{\partial(1/T)}\right]_P = -\frac{\Delta H_a}{R} \quad (6)$$

Similarly, the dependence of $\ln(k^0_{ET})$ on P provides the activation volume[10,14,58,66,67,82–84] *via* eqn (7),

$$\left[\frac{\partial(\ln k^0)}{\partial P}\right]_T = -\frac{\Delta V_a}{RT} \quad (7)$$

Over limited ranges of T and P, the values of the activation parameters are nearly constant (see ESI† for a more full discussion). Table 1 summarizes the values of these parameters which were obtained in this work and elsewhere for Au–SAM–Az junctions.

Fig. 4–6, panels A and B, show the temperature and pressure dependencies of the ET rate constants that were extracted by applying the Marcus model to the voltammograms, which were measured for Au–SAM (n = 4)–Az junctions in contact with different [ch][dhp] blends. Fig. 4 shows an Arrhenius plot, $\ln(k^0)$ *versus* $1/T$, for the aqueous electrolyte (no [ch][dhp] added)[10,14] and the cases of [ch][dhp]–water mixtures of 80, 85 and 90%, w/w (with *ca.* 3.7, 2.6 and 1.7 waters per [ch][dhp]); see Table 1 for more numerical details. Fig. 6 panel A, shows the temperature dependence of the rate constant for mixtures of 50% and 70% (15 and 6.3 waters per [ch][dhp]), which display anomalous behavior, and Fig. 6 panel B, shows the pressure dependence of the rate constant for the matching solution compositions.

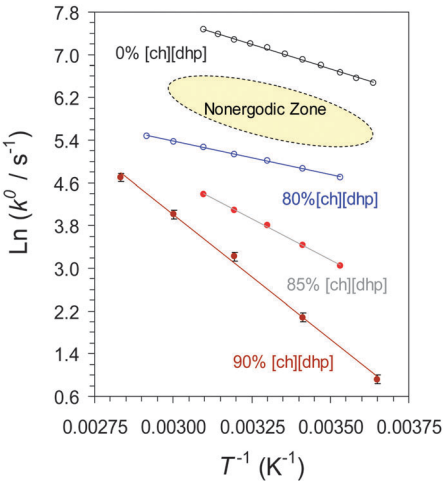

Fig. 4 Arrhenius plots for ET rate constants of Az immobilized at SAM (n = 4) coated Au electrodes, placed in a water-doped and buffered (pH 4.6) protic ionic melt containing 0 (ref. 10), 80 (blue), 85 and 90% w/w [ch][dhp] (from top to bottom). The data for 50 and 70% mixtures fall with the ''Nonergodic Zone'' and display ''anomalous'' Arrhenius plots, see text and Fig. 6, panel A.

Table 1 Kinetic and activation parameters of ET (electron exchange) for Az hydrophobically immobilized on 1-pentanethiol (n = 4) and 1-hexadecanethiol (n = 15) coated Au electrode at pH 4.6 in the absence[10] and presence of [ch][dhp] at concentrations up to 90% (w/w), acetate buffer, pH 4.6; see ESI for the description of the W–IP estimates. The estimates depicted in the 5th column are based on the data published in ref. 36 (see the ESI)

SAM (n), % [ch][dhp] (w/w)	Water/[ch][dhp] ratio (M/M)[c]	k^0, s^{-1} (20 °C, 0.1 MPa)	$\lambda_0(\lambda_{eff})$/eV	η/cP	τ_{eff}/s	ΔH_a/kJ mol^{-1}	ΔV_a/cm^3 mol^{-1}
n = 4 0% [ch][dhp][a]	— 55.6/0	1000 ± 100	0.3 ± 0.03	≈1	3.2×10^{-5}	15.4 ± 2	+1.7 ± 0.3
n = 4 70% [ch][dhp][b]	**6.25 ± 1.25** 16.7/2.8	*270* (mean value)	*~0.3* (mean value)	≈30 (ref. 36)	*1.2×10^{-4}* (mean)	Non-measurable	Non-measurable
n = 4 80% [ch][dhp]	**3.70 ± 0.70** 11.1/3.2	110 ± 20	0.3 ± 0.03	≈440 (ref. 36)	3.0×10^{-4}	10.5 ± 2	~0
n = 4 85% [ch][dhp]	**2.55 ± 0.50** 8.3/3.4	31 ± 5	0.3 ± 0.03	*~4000* (estimated)	1.0×10^{-3}	25.4 ± 3	~0 (Anomaly at 150 MPa)
n = 4 90% [ch][dhp]	**1.65 ± 0.35** 5.6/3.6	8 ± 2	0.3 ± 0.03	*~74 000* (estimated)	4.0×10^{-3}	40.2 ± 5	—
n = 15 0% [ch][dhp][a]	— 55.6/0	1.34 ± 0.15	0.3 ± 0.03	≈1	Non-applicable	7.6 ± 1	−5.1 ± 0.6
n = 15 70% [ch][dhp]	**6.25 ± 1.25** 16.7/2.8	0.85 ± 0.15	0.5 ± 0.10	≈30 (ref. 36)	Non-applicable	13.2 ± 2	−12.2 ± 1.6

[a] Data for the 0% [ch][dhp] case were taken from ref. 10. [b] Data for the 50% [ch][dhp] are not depicted since virtually are indistinguishable from those for the 70% [ch][dhp] case (see text and ESI for details). [c] Errors for the water/[ch][dhp] mole ratio were calculated using the known minimal and maximal density values for pure protic ionic matter (see ESI for details).

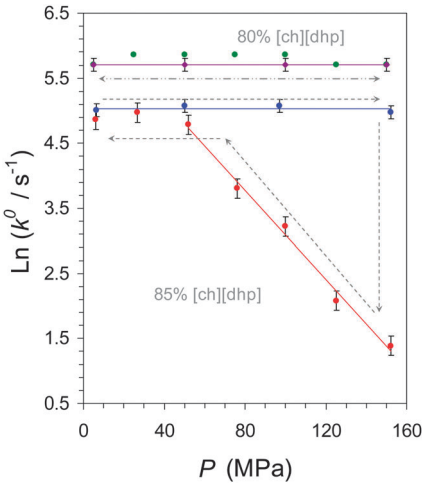

Fig. 5 The pressure dependencies for ET rate constants of Az immobilized at SAM (n = 4) coated coated Au electrodes, placed in a water-doped and buffered (pH 4.6) protic ionic melt containing 80% (top) and 85% (below) [ch][dhp] w/w (all data were collected at 50 °C). The dashed and dashed/dotted arrows show the respective pressure cycling (note a drastic change of the ET constant for the 85% blend at 150 MPa after *ca.* 15 min of additional annealing).

Unlike the case of an aqueous electrolyte[10,14] and despite the overall increased stability of the assemblies with regard to the temperature and pressure variation (*vide supra*), the rate constant data in Fig. 6, panels A and B, show a very peculiar behavior. In particular, the rate constants display hysteresis with T or P cycling, and even the slopes of the plots for $\ln(k^0)$ [in fact, for $\ln(k_{eff})$, see below] *vs.* T^{-1} or P vary. This behavior was observed for multiple different samples and scans (see ESI† for further details). The linearity, reversibility, and reproducibility were restored for the case of a 3.7 water–[ch][dhp] blend, see Fig. 4 and 5; however, a 2.5 water–[ch][dhp] blend exhibited another type of irregularity upon a pressure increase to 150 MPa (with a whole series performed at 323 K). After the standard 30 min of annealing at 150 MPa to allow system equilibration and then performing the first set of voltammetry measurements, it was found that a further 15 min of annealing at 150 MPa led to voltammograms with a much larger peak separation, which correlated to a sudden 38-fold drop in the rate constant (*vide infra*). Upon the subsequent lowering of pressure, the voltammograms gradually returned to a smaller peak separation and the high rate constant value (as found at the very beginning of a pressure cycle), Fig. 5. The data are suggestive of a pressure-triggered reversible conformational transformation within the assemblies. Seemingly, the system is maintained in a metastable state as the pressure increases from 0.1 MPa to 150 MPa, and the transition occurs abruptly during the course of annealing (see text below and ESI† for further details).

Interplay of friction-controlled and nonergodic kinetic motifs

In earlier work on Au–SAM–Az aqueous electrolyte junctions, we showed that the electron transfer mechanism falls within the dynamically-controlled regime for thin SAMs.[10,14] In the present work, we examine these same junctions [pentanethiol (n = 4) SAMs] and vary the parameter $\nu_{eff}(1/\tau_{eff})$ through the change of solution composition, temperature, and pressure. Importantly, the dynamical arrest (nonergodicity) and accompanying kinetic effects should be even more pronounced for short-range (dynamically-controlled) ET in glass-forming media, for which the broad spectrum of slowly relaxing degrees of freedom directly determine the rate constant through the pre-exponential term of the rate equation, eqn (3) (in contrast to long-range ET that is perceptive to the reactive mode freezing–unfreezing solely through the parameter λ_{eff}[18,38–42,58]).

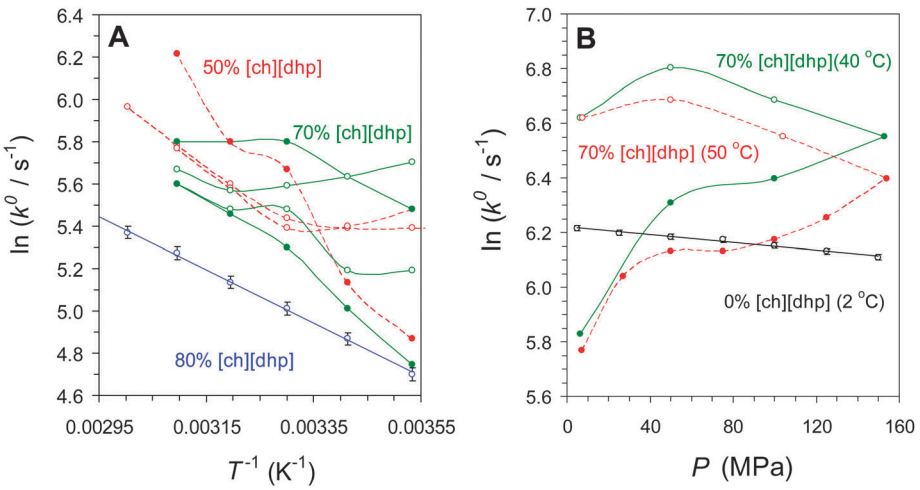

Fig. 6 (A) Arrhenius plots for ET rate constants of Az immobilized at SAM (n = 4) coated Au electrodes placed in a water-doped and buffered (pH 4.6) protic ionic melt containing 50% (dashed curves) and 70% (solid curves) ([ch][dhp]) w/w. Open and filled symbols indicate cycles with a temperature increase and decrease, respectively. A linear Arrhenius plot below represents a system with 80% [ch][dhp] depicted for the comparison. (B) The pressure dependencies for the same assembly placed in a water-doped and buffered (pH 4.6) protic ionic melt containing 70% ([ch][dhp]) w/w; the data were collected at 50 °C (dashed curves) and 40 °C (solid curves), respectively. Open and filled symbols indicate cycles with the pressure increase and decrease, respectively. The linear pressure dependence for a reference system with no [ch][dhp] added (recorded at 2 °C, ref. 10) is also depicted for comparison (no reverse cycle was possible in that case).

Surprisingly, the value of λ_{eff}, which is extracted by applying the Marcus model to the CV data covering overvoltages of "normal" behavior, remains virtually constant for the cases of 0, 50, 70, 80, 85 and 90% blends (excluding the anomalous deviations at sufficiently high overvoltages in the two latter cases, under 150 MPa and below room temperature conditions). This feature seems to contradict the predictions regarding the lowering of λ_{eff} due to the nonergodic aspect.[18,38,41,42] However, one should bear in mind that the resulting (effective) Gibbs energy wells that shape λ_{eff} are almost equally contributed by the fast, statistically independent harmonic modes, and by slow, cooperatively relaxing, (dissipative) modes, latter being liable to inharmonic alterations. Seemingly, under moderate experimental conditions (ample water content, room temperature, ambient pressure, low energy gaps), both of them tend to display linear or, at least, quasi-linear medium response patterns.[16,39–41,54,55] Obviously, a range for the variation of k^0 *versus* the variable water content, T and P in this work was too small to 'freeze out' the fast modes (which, presumably, predominantly determine the value of λ_{eff} at low overpotentials). This explanation is consistent with previous work[58] that examined Au–SAM (n)–IL–Fc assemblies (Fc, ferrocene; n = 2 to 18), where a 50% decrease in λ_{eff} was found. In that case k^0 was varied by 10^5-fold through the variation of V_{AB} in the nonadiabatic limit, as compared to the current case of only a 100-fold change in k^0, Table 1. Furthermore, the system's slowest cooperatively relaxing degrees of freedom which directly determine the value of the rate constant through the parameter ν_{eff} (eqn (3) and (4)), in a dynamically-controlled regime,[10,14] initially contributing to λ_{eff} mostly harmonically (note the dual contribution of slow modes to k^0 – *via* ν_{eff} and λ_{eff}!) tend to behave increasingly nonlinearly when approaching harsh glassy conditions. Indeed, nonlinearity of the medium response (departure of Gibbs energy wells from the harmonic shape) should start to show up notably at larger fluctuational deviations from respective equilibrium positions, required at larger overvoltages (see the next subsection for further details).

Another surprising feature of the Au–SAM (n = 4)–Az junctions is the remarkably low values of the effective frequency, ν_{eff}; *i.e.*, a large value for the effective relaxation time, τ_{eff}, which is found to be 32 μs for the case of the aqueous electrolyte and as long as 4 ms for the 90% [ch][dhp] (at 20 °C, 0.1 MPa, see Table 1). It is noteworthy that the "starting" value of τ_{eff} for Az is *ca.* two orders of magnitude larger than that deduced for the surface-confined cytochrome *c* (CytC).[4,8,14] This fact is likely to reflect the difference in the details of their confinement to the SAM film;[4,8,14] indeed, as demonstrated for CytC, the SAM confinement contributes to the effective relaxation time.[14,65] One may suppose that for the Au–SAM–Az junctions in contact with the 15 and 6.3 W–IP blends, the relaxation spectrum contributing to ν_{eff} (determining k^0 through eqn (1) and (5)), is mostly related to protein–PIM–water modes that are of the moderately cooperative β-relaxation (Johary–Goldstein) type (see also the next subsection).[20,24–26] This spectrum would be sensitive to the melt composition and presumably shifts to a slower timescale window with a decrease of the water content, leading to a decrease of the ET rate constant through the parameter ν_{eff}. With a decrease of the water content in the bulk solution (melt) and at the protein/solution interface, the cooperativity of the contributing ("unfrozen") slowest relaxation modes should increase (a manifold of β-relaxations gradually or with small steps would merge into a few α-relaxations, see ref. 20 and 24–26), leading to the increase of τ_{eff} (decrease in ν_{eff}). As a result, the system may leave the nonergodic zone in which the τ_{eff} crosses the respective instrumental time domain (see Fig. 4).

Interplay of friction-controlled and nonlinear (glassy) kinetic motifs

Consider the results for the impact of pressure on k^0 for the case of a 2.6 water–[ch][dhp] blend (50 °C). An analysis of the scan rate dependence for the respective redox peak shift shows significant deviations from the Marcus model. Fig. 2 (panel A) and 3 (panel A), and 7 show that the conventional Marcus model can describe the peak shift for the system before the pressure-induced abrupt transition (seemingly, to the glass-like state, *vide supra*), but after the transition, at higher scan rates (that is, high overvoltages), deviates from it very strongly. Similarly the data collected around and below room temperature for the 1.7 water–[ch][dhp] blend (see Fig. 3, panel B, and 7) show significant deviations from the Marcus model at high scan rates (high overvoltages). Before the sudden P-induced, and gradual T-induced anomalous transitions for the 2.6 and 1.7 water–[ch][dhp] blends, respectively, the experimental data can be fitted by a single Marcus-type curve (based on eqn (1) and (2)) with λ_{eff} = 0.3 eV; whereas after the transition, only the initial portion of the experimental points fall on the same curve and the rest of the data cannot be fitted by any reasonable Marcus-type curve (see Fig. 3, panels A and B). This clear failure

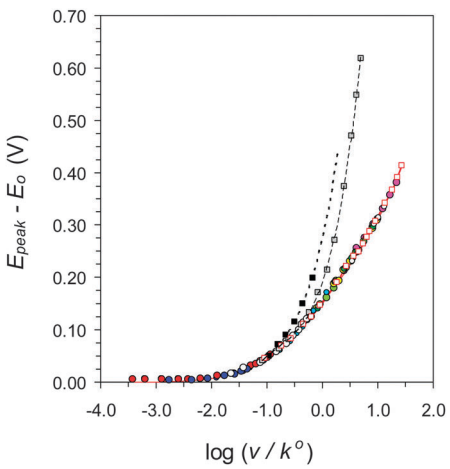

Fig. 7 A muster plot for the CV peak potential deviations (from the midpoint potential) as a function of the scaled scan rate (all symbols), for data reported in ref. 10, and this work (collected throughout 273–353 K and 0.1–150 MPa), including the "anomalous" records presented in Fig. 3; throughout, the anodic peak is shown only for clarity. Most data can be satisfactorily fitted by the Marcus model through a single curve resembling λ = 0.3 eV. Deviations from the "universal" curve are evident for the data of Fig. 3A (black squares) and B (gray squares) at overvoltages above *ca.* 0.05 and 0.15 V, respectively. The dashed curves are drawn to guide the eye only.

of the Marcus model implies that, as already mentioned above, parabolic energy wells (a result of linear response) may not apply. The fact that these data deviate so strongly from the conventional picture indicates that this anomaly, the 38-fold sudden drop of the k^0 value (Fig. 3, panel A, and 7) and the gradual 44-fold T-induced transformation (Fig. 3, panel B, and 7), are caused by another kind of breakdown [of type (b)] that is distinct from the nonergodicity signature [of type (a) above]. Why would the T-related irregularity (b) occur gradually, presumably without involvement of metastable states, whereas the P-related one [again the (b) type] is abrupt? This difference may result from the different standard equilibration times that are used for the temperature scans, as compared to the pressure variation scans.

In addition to the pentanethiol assemblies, this study employed an Au–SAM–Az junction that is composed of a hexadecanethiol (n = 15) SAM, which falls within the non-adiabatic regime,[10,14] as a reference system (see Table 1 and ESI†). Fig. 7 shows the simultaneous fitting of the experimental voltammogram's oxidation peak potential deviations as a function of the scaled scan rate (all symbols), reported in Fig. 2 of ref. 10, and in this work, Fig. 2 (panels A and B), and 3 (panels A and B; the anodic peaks are only shown throughout for the presentation quality). The data with comparable scaled overvoltages (from 0.2 to 0.4 V) are taken from the previous[10] and present (open red squares) work for Az immobilized on a n-hexadecanethiol (n = 15) SAM with no [ch][dhp] added and altogether fitted by the Marcus model (red solid line), yielding a single value of λ = 0.3 eV throughout. Deviations from the "universal" curve are evident for the data of Fig. 3, panel A (black squares) and 3, panel B (gray squares) at overvoltages above *ca.* 0.1 and 0.15 V, respectively, connected by the dotted and dashed curves, respectively (drawn to guide the eye). Interestingly, results obtained from thicker SAMs for the case of a 6.3 water–[ch][dhp] (experimentally allowing for similar overvoltages) do not exhibit any anomalies in the temperature and pressure dependence, nor any deviation from the quadratic (Marcus) free energy model. However, in line of our interpretations given above, these dissimilarities can be attributed to the exclusion of the type (b) irregularity due to the lack of glass-forming conditions (the PIM concentration of only 70% w/w *versus* 85 and 90% w/w) in case of the Au–SAM (n = 15)–Az assembly compared to the Au–SAM (n = 4)–Az one.

According to Mallamance *et al.*,[22,23] glassy dynamics starts to show up at the "dynamic crossover temperature", much higher above the "calorimetric glass transition temperature" (see, *e.g.* ref. 17, 20 and 21), at which the system's viscosity approaches $\sim 10^3$ poise. Jansson *et al.*[25,26] found for myoglobin-based glassy systems that starting from *ca.* 180 K (the glass transition temperature), up to 250–300 K,[25,26] a few of the slowest relaxation times for several triple protein–water–plasticizer mixtures exhibit nearly linear Arrhenius dependencies, yielding values of $\Delta H_a^{(R)}$ which are comparable to that found in this work for a friction-controlled ET in the 90% [ch][dhp] blend within the temperature range of 273–353 (ΔH_a = 40.2 kJ mol^{-1}; Table 1). In the abovementioned studies the relaxation was probed with broadband dielectric spectroscopy and the glass transition was revealed through differential scanning calorimetry.[25,26] Quite in parallel, Capaccioli *et al.*[24] reported that the values for $\tau_{eff}^{(R)}$ and $\Delta H_a^{(R)}$ (implying the slowest relaxation process itself) approach the critical limits that are common for many glass-forming materials (including the triple protein–water–plasticizer mixtures) well above the temperature for an onset of the calorimetrically detectable glass transition.[24] Obviously, the pre-conditioned extra confinement at the SAM interface, with the SAM to some extent representing the semi-solid environment, should additionally facilitate the glassy behavior for Az. Accordingly, one could conclude that the viscosity limit for entering the glassy dynamics zone (10^3 poise[22,23]) was more than enough met at most extreme conditions used in this study (the most concentrated [ch][dhp], highest P, moderately low T), hence these systems definitely were approaching the glassy state, which is unprecedented for a surface-confined and fully functionalized redox protein. Presumably, this fact brings about the anomaly of nonlinear medium response. Finally, Fig. 8 depicts the situation in which a steepening of the free energy well's wings may cause a severe deviation from the free energy relationship predicted by the Marcus model.[54,55,69] This Figure sketches the situation that can be used to understand the data in Fig. 3, panels A and B, and 7. The manifold of potential surfaces matching the electron's virtually inoperative states in the electrode (below the Fermi level; see *e.g.*, ref. 85) is not shown for clarity.

The above discussed mechanistic motifs that presumably show up as observed dramatic kinetic manifestations are

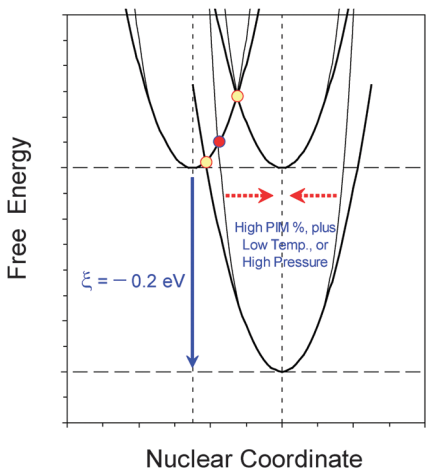

Fig. 8 Schematic presentation of free energy (FE) profiles for the electron exchange between Az and a Au electrode at Au–SAM–Az–PIM junctions for the case of zero overpotential and −0.2 V overpotential. This drawing illustrates the impact of a hypothetical increase of the FE curvature (from harmonic to higher at larger deviations from the equilibrium) at high [ch][dhp] concentrations combined with the application of high pressure and/or low temperature. The small open circles indicate transition points at zero and −0.2 V overpotentials when the FE terms are still harmonic. The filled circle indicates a transition point at −0.2 V overpotential provided that the final FE term is not harmonic any more (taken as quartic here; see text for the detailed discussion). The manifold of FE surfaces matching the electron's virtually inoperative states in the electrode (below the Fermi level)[85] is not shown for clarity of presentation.

essentially distinct from those which might be potentially connected to the hypothetical deviations from the pattern set by the conventional Franck–Condon approximation.[86–88] These kinds of motifs have been considered theoretically and shown that they could be actual for both the nonadiabatic (long-range, electronically controlled)[86,88] and adiabatic (short-range, dynamically controlled)[87] ET processes. It seems that so called ''non-Condon'' motifs may show up for ET processes with either very small[86,88] or exceedingly large[87] values of V_{AB}, respectively. For the latter case, application of the ''improved Condon approximation'' indicated a larger well splitting, hence greater deformation of diabatic (''channel'') Gibbs energy terms, compared to the case predicted by the ''rough Condon approximation''.[87] The expected effect is certainly different from the nonlinear response motif related to the energy well steepening discussed above. Moreover, the processes of our foremost interest (ET within Au–SAM (n = 4)–Az junctions), encompass the rather modest value of V_{AB} (see, *e.g.*, ref. 14, 58 and 89; however, assuring the occurrence of the dynamically controlled regime[10,14]), hence do not fall within the range of values providing considerable Franck–Condonian consequences.

Experimental

Materials

Highly purified *P. aeruginosa* azurin was purchased from Sigma and was used without further purification. The starting material for the buffer doped [ch][dhp] was purchased from Ionic Liquids Technologies (Iolitech, GmbH) and was used as received. Alkanethiols, highest purity commercially available, [1-pentanethiol (Acros), and 1-hexadecanethiol (Aldrich)] were used as received. The buffer components, ultrapure 5 M ammonium acetate and $HClO_4$ (70%) were from Fluka. The Az films were prepared according to published procedures. All the PIM blends were adjusted to have pH 4.6 (see ref. 10 and ESI† for details).

Instrumentation and data processing

The Az film voltammetry was carried out with an Autolab Electrochemical Analyzer PGSTAT 30. The pressure vessel and electrochemical cell have been described elsewhere (for some distinctive details see the ESI†).[10,56,57,66,67] GPES software was used for the primary data analysis and the ''post-measurement'' Ohmic potential drop corrections for the experimental CV response (see ref. 10, 56 and 66 and ESI† for the procedural details). The conductivity of all aqueous [ch][dhp] blends (work solutions) was checked by standard instrumentation (see ESI†). It was found that conductivity of all solutions was high enough that the *iR* drop correction had no significant impact on the voltammetric data (see ESI†). Nevertheless, the post-measurement software-aided corrections were made (see ref. 10 and ESI†), hence the results reported in this paper are essentially free of Ohmic potential drop errors.

According to ref. 90–92, the features of CV curves, other than the Faradaic peak positions, such as the peak half-height widths (FWHM), may carry useful information regarding fine mechanistic details for redox-active species functionalized at derivatized electrodes. We have performed preliminary analysis of our CV data regarding this aspect, and found that under the ''standard'' experimental conditions[10] (in the absence of the [ch][dhp] component) the values for FWHMs were very close to respective theoretical ones (with an accuracy of 1 to 2%, also including the temperature aspect). The presence of [ch][dhp] at the highest concentration of 95% w/w, led to the increase of FWHMs such to exceed ''ideal'' values by 10–20%. However, FWHMs were not affected by the *P*- and *T*-induced transitions to ''anomalous'' large peak-separations, presumably due to the non-Marcussian (nonlinear) medium response discussed above. The rather modest peak-broadening effect observed in this work is comparable to one (however, being three times less) found by Armstrong *et al.*[91,92] for a single-electron exchange with a ''7Fe'' ferrodoxin at the pyrolytic graphite edge electrode at cryogenic temperatures, ascribed to a factor of ''inhomogeneous freezing'' of the medium for a surface-confined Az population around −70 °C. We believe that some effects of ''inhomogeneous freezing'' of Az may take place in our case as well, however this effect, if it really exists, should be independent of (and minor as compared to) the two firmly pronounced kinds of kinetic anomalies discussed above; and hence cannot affect our major conclusions.

It should be mentioned that the knowledge of ''true'' values of E_o for immobilized redox species (in this particular case, Az), is not required for the extraction of kinetic parameters through the CV data analysis within the framework of a Marcus model (just keeping $E_{o(eff)}$ stable during the sweep rate variation suffices).[60–62] For the determination of E_o, in our case, severe methodological restrictions of two kinds, connected with a lack of the applicability of ''non-isothermal''[81] and corresponding ''non-isobaric'' conditions for our home-made high-pressure cell and subsequent proper calibration of a quasi-reference electrode,[93,94] would emerge (see ESI†). An impact of the [ch][dhp]-rich medium for Az and other redox proteins on their E_o will be considered thoroughly in a separate study.

Conclusions

In summary, sandwich-like assemblies composed of gold-deposited alkanethiol SAMs and irreversibly adsorbed films of a redox-active protein azurin were placed in contact with semi-solid electrolytes, buffered protic ionic melts of variable doping water content. The fast-scan voltammetry studies of biological ET within the semi-solid environment (presumably, approaching the glassy state; made available in this work just below room-temperature or under high-pressure conditions) revealed the need to consider two novel distinctive kinetic motifs that manifest as ''irregularities'' when the electron transfer is treated in the framework of a ''traditional'' Marcus-like formalism. From an experimental standpoint, the two anomalies are quite distinct, and hence are interpreted as arising from nonergodic and nonlinear kinetic effects that have been predicted notionally for complex environments. These effects are taken to be different manifestations of a primary breakdown in the time-separation

and quasi-static views of medium effects on electron transfer, respectively. Consequently, this work seems be a first systematic effort in which three modern physical concepts, encompassing: (a) dynamically controlled (adiabatic) interfacial ET; (b) the medium's nonergodic response (dynamically arrested ET); and (c) the medium's nonlinear response (nonparabolic free energy terms for ET), were invoked to experimentally uncover and elucidate the novel mechanistic peculiarities for a special case of biological ET within the mimetic (biologically relevant) complex environments. It should also be mentioned here that since almost the whole experimental outcome of this work turned out to be unprecedentedly peculiar, its adequate, at least tentative, interpretation necessitated involvement of a comprehensive blend of up-to-date theoretical models/concepts which applicability, *per se*, however was shown here to be somewhat restricted, suggestive of the further systematic theoretical elaboration. Therefore, the specific conclusions drawn above, certainly have rather speculative character, and are to be subjected to severe verification by complementary experimental methods in the future.

Acknowledgements

Research grants from the Volkswagen Foundation, Germany, I/83 395 and I/85 642 (R. v. E., D. E. K., T. D. D. and T. T.), Rustaveli National Science Foundation, Georgia, GNSF/ST08/2-374 and FR/771/7-230/11 (D. E. K., T. D. D. and T. T.), the Deutsche Forschungsgemeinschaft (DFG) as part of SFB 583 on ''Redox-active Metal Complexes'' (R. v. E.) are kindly acknowledged. D. H. W. acknowledges financial support from the US National Science Foundation (CHE 1059037). D. E. K acknowledges senior fellowships from the Alexander von Humboldt Foundation, Germany (2010, 2013) and the Fulbright Foundation, USA (2011–2012). T. D. D. acknowledges a senior fellowship from the Deutsche Akademische Austauschdienst (DAAD), Germany (2011). The authors are grateful to Harry Gray and Dmitry Matyushov for valuable exchanges.

References

1 Q. Chi, J. Zhang, J. E. T. Andersen and J. Ulstrup, *J. Phys. Chem. B*, 2001, **105**, 4669–4679.
2 L. J. C. Jeuken, J. P. McEvoy and F. A. Armstrong, *J. Phys. Chem. B*, 2002, **106**, 2304–2313.
3 Q. Chi, O. Farver and J. Ulstrup, *Proc. Natl. Acad. Sci. U. S. A.*, 2005, **102**, 16203–16208.
4 D. E. Khoshtariya, J. Wei, H. Liu, H. Yue and D. H. Waldeck, *J. Am. Chem. Soc.*, 2003, **125**, 7704–7714.
5 K. Niki, W. R. Hardy, M. G. Hill, H. Li, J. R. Sprinkle, E. Margoliash, K. Fujita, R. Tanimura, N. Nakamura, H. Ohno, J. H. Richards and H. B. Gray, *J. Phys. Chem. B*, 2003, **107**, 9947–9949.
6 H. B. Gray and J. R. Winkler, *Proc. Natl. Acad. Sci. U. S. A.*, 2005, **102**, 3534–3539.
7 D. H. Murgida and P. Hildebrandt, *Acc. Chem. Res.*, 2004, **37**, 854–861.
8 H. Yue, D. E. Khoshtariya, D. H. Waldeck, J. Grohol, P. Hildebrandt and D. H. Murgida, *J. Phys. Chem. B*, 2006, **110**, 19906–19913.
9 K. Yokoyama, B. S. Leigh, Y. Sheng, K. Niki, N. Nakamura, H. Ohno, J. R. Winkler and H. B. Gray, *Inorg. Chim. Acta*, 2008, **361**, 1095–1099.
10 D. E. Khoshtariya, T. D. Dolidze, M. Shushanyan, K. Davis, D. H. Waldeck and R. Van Eldik, *Proc. Natl. Acad. Sci. U. S. A.*, 2010, **107**, 2757–2762.
11 H. K. Ly, M. A. Marti, D. F. Martin, D. Alvarez-Paggi, W. Meister, A. Kranich, I. M. Weidinger, P. Hildebrandt and D. H. Murgida, *ChemPhysChem*, 2010, **11**, 1225–1235.
12 S. Monari, G. Battistuzzi, C. A. Bortolotti, S. Yanagisawe, K. Sato, C. Li, I. Salard, D. Kostrz, M. Borsari, A. Ranieri, C. Dennison and M. Sola, *J. Am. Chem. Soc.*, 2012, **134**, 11848–11851.
13 H. B. Gray and J. R. Winkler, *Biochim. Biophys. Acta, Bioenerg.*, 2010, **1797**, 1563–1572.
14 D. H. Waldeck and D. E. Khoshtariya, in *Modern aspects of Electrochemistry. Applications of Electrochemistry and Nanotechnology in Biology and Medicine*, No. 52, ed. N. Elias, Springer, New York, 2011, pp. 105–241.
15 H. Frauenfelder and P. G. Wolynes, *Science*, 1985, **229**, 337–345.
16 J. N. Onuchic and P. G. Wolynes, *J. Chem. Phys.*, 1993, **98**, 2218–2224.
17 C. A. Angell, *Science*, 1995, **267**, 1924–1935.
18 B. M. Hoffman and M. A. Ratner, *Inorg. Chim. Acta*, 1996, **243**, 233–238.
19 F. A Tezcan, B. R. Crane, J. R. Winkler and H. B. Gray, *Proc. Natl. Acad. Sci. U. S. A.*, 2001, **98**, 5002–5006.
20 H. Frauenfelder, G. Chen, J. Berendzen, P. W. Fenimore, H. Jansson, B. H. McMahon, I. R. Store, J. Swenson and R. D. Young, *Proc. Natl. Acad. Sci. U. S. A.*, 2009, **106**, 5129–5134.
21 W. Doster, *Biochim. Biophys. Acta, Proteins Proteomics*, 2010, **1804**, 3–14.
22 F. Mallamance, C. Branca, C. Corsaro, N. Leone, J. Spooren, S.-H. Chen and H. E. Stenley, *Proc. Natl. Acad. Sci. U. S. A.*, 2010, **107**, 22457–22462.
23 F. Mallamance, C. Corsaro, H. E. Stenley and S.-H. Chen, *Eur. Phys. J. E*, 2011, **34**, 94.
24 S. Capaccioli, K. L. Ngai, S. Ancherbak, P. A. Rolla and N. Shinyashiki, *J. Non-Cryst. Solids*, 2011, **357**, 641–654.
25 H. Jansson and J. Swenson, *Biochim. Biophys. Acta, Proteins Proteomics*, 2010, **1804**, 20–26.
26 H. Jansson, R. Bergman and J. Swenson, *J. Phys. Chem. B*, 2011, **115**, 4099–4109.
27 A. K. Yagati, S.-U. Kim, J. Minc and J.-W. Choi, *Biosens. Bioelectron.*, 2009, **24**, 1503–1507.
28 M. L. Vargo, C. P. Gulka, J. K. Gerig, C. M. Manieri, J. D. Dattelbaum, C. B. Marks, N. T. Lawrence, M. L. Trawick and M. C. Leopold, *Langmuir*, 2010, **26**, 560–569.
29 L. Sepunaru, I. Pecht, M. Sheves and D. Cahen, *J. Am. Chem. Soc.*, 2011, **133**, 2421–2423.
30 A. G. Lee, *Biochim. Biophys. Acta, Biomembr.*, 2004, **1666**, 62–87.

31 A.-N. Bondar and S. H. White, *Biochim. Biophys. Acta, Biomembr.*, 2004, **1818**, 942–950.
32 J.-P. Belieres and C. A. Angell, *J. Phys. Chem. B*, 2007, **111**, 4926–4937.
33 U. A. Rana, P. M. Beyley, R. Vijayaraghavan, P. Howlett, D. R. MacFarlane and M. Forsyth, *Phys. Chem. Chem. Phys.*, 2010, **12**, 11291–11298.
34 K. Fujita, R. D. MacFarlane and M. Forsyth, *Chem. Commun.*, 2005, 4804–4806.
35 D. Constatinescu, C. Herrmann and H. Weingärtner, *Phys. Chem. Chem. Phys.*, 2010, **12**, 1756–1763.
36 K. Fujita and H. Ohno, *Biopolymers*, 2010, **93**, 1093–1099.
37 K. D. Weaver, R. M. Vrikkis, M. P. Van Vorst, J. Trullinger, R. Vijayaraghavan, D. M. Foureau, I. H. McKillop, D. R. MacFarlane, J. K. Krueger and G. D. Elliott, *Phys. Chem. Chem. Phys.*, 2012, **14**, 790–801.
38 V. Kapko and D. V. Matyushov, *J. Phys. Chem. B*, 2006, **110**, 13184–13194.
39 D. N. LeBard and D. V. Matyushov, *J. Phys. Chem. B*, 2008, **112**, 5218–5227.
40 D. N. LeBard and D. V. Matyushov, *Phys. Chem. Chem. Phys.*, 2010, **12**, 15335–15348.
41 D. V. Matyushov, *J. Phys. Chem. B*, 2011, **115**, 10715–10724.
42 D. V. Matyushov, *J. Phys. Chem. Lett.*, 2012, **3**, 1644–1648.
43 R. A. Marcus, *J. Chem. Phys.*, 1965, **43**, 679–701.
44 R. R. Dogonadze and A. M. Kuznetsov, *Prog. Surf. Sci.*, 1975, **6**, 1–41.
45 R. A. Marcus and N. Sutin, *Biochim. Biophys. Acta, Rev. Bioenerg.*, 1985, **811**, 265–322.
46 L. D. Zusman, *Chem. Phys.*, 1987, **112**, 53–59.
47 J. D. Morgan and P. G. Wolynes, *J. Phys. Chem.*, 1987, **91**, 874–883.
48 H. Sumi and R. A. Marcus, *J. Chem. Phys.*, 1986, **84**, 4894–4914.
49 I. Rips and J. Jortner, *J. Chem. Phys.*, 1987, **87**, 2090–2104.
50 A. K. Mishra and D. H. Waldeck, *J. Phys. Chem. C*, 2009, **113**, 17904–17914.
51 R. G. Palmer, *Adv. Phys.*, 1982, **31**, 669–735.
52 D. L. Stein and C. M. Newman, *Phys. Rev. E: Stat. Phys., Plasmas, Fluids, Relat. Interdiscip. Top.*, 1995, **51**, 5228–5238.
53 J. C. Mauro, P. K. Gupta and R. J. Loucks, *J. Chem. Phys.*, 2007, **126**, 184511.
54 O. Miyashita, J. N. Onuchic and P. G. Wolynes, *Proc. Natl. Acad. Sci. U. S. A.*, 2003, **100**, 12570–12575.
55 L. Meinhold, J. C. Smith, A. Kitao and A. H. Zewail, *Proc. Natl. Acad. Sci. U. S. A.*, 2007, **104**, 17261–17265.
56 G. P. Wiederrecht, W. A. Svec and M. R. Wasielewski, *J. Phys. Chem. B*, 1999, **103**, 1386–1389.
57 M. Tachiya and A. V. Barzykin, *Chem. Phys.*, 2005, **319**, 222–225.
58 D. E. Khoshtariya, T. D. Dolidze and R. van Eldik, *Chem.–Eur. J.*, 2009, **15**, 5254–5262.
59 C. E. D. Chidsey, *Science*, 1991, **251**, 919–922.
60 K. Weber and S. E. Creager, *Anal. Chem.*, 1994, **66**, 3164–3172.
61 L. Tender, M. T. Carter and R. W. Murrey, *Anal. Chem.*, 1994, **66**, 3173–3181.
62 K. Weber, L. Hockett and S. E. Creager, *J. Phys. Chem. B*, 1997, **101**, 8286–8291.
63 T. D. Dolidze, D. E. Khoshtariya, D. H. Waldeck, J. Macyk and R. van Eldik, *J. Phys. Chem. B*, 2003, **107**, 7172–7179.
64 D. E. Khoshtariya, T. D. Dolidze, S. Seifert, D. Sarauli, G. Lee and R. van Eldik, *Chem.–Eur. J.*, 2006, **12**, 7041–7056.
65 T. D. Dolidze, S. Rondinini, A. Vertova, D. H. Waldeck and D. E. Khoshtariya, *Biopolymers*, 2007, **87**, 68–73.
66 T. D. Dolidze, D. E. Khoshtariya, P. Illner, L. Kulisiewicz, A. Delgado and R. van Eldik, *J. Phys. Chem. B*, 2008, **112**, 3085–3100.
67 D. E. Khoshtariya, T. D. Dolidze and R. van Eldik, *Phys. Rev. E: Stat., Nonlinear, Soft Matter Phys.*, 2009, **80**, 065101.
68 N. G. Goguadze, D. E. Khoshtariya, J. M. Hammerstad-Pedersen and J. Ulstrup, *Eur. J. Biochem.*, 1991, **200**, 423–429.
69 B. Gavish and S. Yedgar, in *Protein–Solvent Interactions*, ed. R. B. Gregory, Marcel Dekker, New York, 1995, pp. 343–373.
70 M. Cascella, A. Magistrato, I. Tavernelli, P. Carloni and U. Rothlisberger, *Proc. Natl. Acad. Sci. U. S. A.*, 2006, **103**, 19641–19646.
71 J. A. Hegler, P. Weinkam and P. G. Wolynes, *HFSP J.*, 2008, **2**, 307–313.
72 M. Shushanyan, D. E. Khoshtariya, T. Tretyakova, M. Makharadze and R. van Eldik, *Biopolymers*, 2011, **95**, 852–870.
73 T. Tretyakova, M. Shushanyan, T. Partskhaladze, M. Makharadze, R. van Eldik and D. E. Khoshtariya, *Biophys. Chem.*, 2013, **175–176**, 17–27.
74 Y. Shim and H. J. Kim, *J. Phys. Chem. B*, 2007, **111**, 4510–4519.
75 R. M. Linden-Bell, *J. Phys. Chem. B*, 2007, **111**, 10800–10806.
76 M.-M. Huang and H. Weingärtner, *ChemPhysChem*, 2008, **9**, 2172–2173.
77 M.-M. Huang, Y. Jiang, P. Sasisanker, G. W. Driver and H. Weingärtner, *J. Chem. Eng. Data*, 2011, **56**, 1494–1499.
78 K. A. Kurnia, M. M. Taib, A. Mutalib and T. Murugesan, *J. Mol. Liq.*, 2011, **159**, 211–219.
79 C. La Rosa, D. Milardi, D. Grasso, R. Guzzi and L. Sportelli, *J. Phys. Chem.*, 1995, **99**, 14864–14870.
80 P. Cioni, *Biophys. J.*, 2006, **91**, 3390–3396.
81 S. Monari, G. Battistuzzi, C. Dennison, M. Borsari, A. Ranieri, M. J. Siwek and M. Sola, *J. Phys. Chem. C*, 2010, **114**, 22322–22329.
82 R. van Eldik, T. Asano and W. J. Le Noble, *Chem. Rev.*, 1989, **89**, 549–688.
83 R. van Eldik, *Adv. Chem.*, 1998, **254**, 315–330.
84 T. W. Swaddle, *Chem. Rev.*, 2005, **105**, 2573–2608.
85 Q. Chi, J. Zhang, P. S. Jensen, H. E. M. Christensen and J. Ulstrup, *Faraday Discuss.*, 2006, **131**, 181–195.
86 I. Daizadeh, E. M. Medvedev and A. A. Stuchebrukhov, *Proc. Natl. Acad. Sci. U. S. A.*, 1997, **94**, 3703–3708.

87 A. M. Kuznetsov, V. V. Sokolov and J. Ulstrup, *J. Electroanal. Chem.*, 2001, **502**, 36–46.
88 S. S. Skourtis, I. A. Balabin, T. Kawatsu and D. N. Beratan, *Proc. Natl. Acad. Sci. U. S. A.*, 2005, **102**, 3552–3557.
89 D. E. Khoshtariya, T. D. Dolidze, L. D. Zusman and D. H. Waldeck, *J. Phys. Chem. A*, 2001, **105**, 1818–1829.
90 E. Laviron, in *Electroanalytical Chemistry*, ed. A. J. Bard, Marcel Dekker, New York, 1982, vol. 12, pp. 53–157.
91 J. P. McEvoy and F. A. Armstrong, *Chem. Commun.*, 1999, 1635–1636.
92 F. A. Armstrong, R. Camba, H. A. Heering, J. Hirst, L. J. C. Jeunken, A. K. Jones C. Leger and J. P. McEvoy, *Faraday Discuss.*, 2000, **116**, 191–203.
93 J. Zhang and A. M. Bond, *Anal. Chem.*, 2003, **75**, 6938–6948.
94 A. A. J. Torriero, J. Sunarso and P. C. Howlett, *Electrochim. Acta*, 2012, **82**, 60–68.